Deep Drilling into the Chesapeake Bay Impact Structure

G. S. Gohn, *et al.*

Science **320**, 1740 (2008);
DOI: 10.1126/science.1158708

Science (print ISSN 0036-8075; online ISSN 1095-9203) is published weekly, except the last week in December, by the American Association for the Advancement of Science, 1200 New York Avenue NW, Washington, DC 20005.

Deep Drilling into the Chesapeake Bay Impact Structure

G. S. Gohn,[1]* C. Koeberl,[2] K. G. Miller,[3] W. U. Reimold,[4] J. V. Browning,[3] C. S. Cockell,[5] J. W. Horton Jr.,[1] T. Kenkmann,[4] A. A. Kulpecz,[3] D. S. Powars,[1] W. E. Sanford,[1] M. A. Voytek[1]

Samples from a 1.76-kilometer-deep corehole drilled near the center of the late Eocene Chesapeake Bay impact structure (Virginia, USA) reveal its geologic, hydrologic, and biologic history. We conducted stratigraphic and petrologic analyses of the cores to elucidate the timing and results of impact-melt creation and distribution, transient-cavity collapse, and ocean-water resurge. Comparison of post-impact sedimentary sequences inside and outside the structure indicates that compaction of the crater fill influenced long-term sedimentation patterns in the mid-Atlantic region. Salty connate water of the target remains in the crater fill today, where it poses a potential threat to the regional groundwater resource. Observed depth variations in microbial abundance indicate a complex history of impact-related thermal sterilization and habitat modification, and subsequent post-impact repopulation.

The Chesapeake Bay impact structure (CBIS) is among the largest and best preserved of the known terrestrial impact structures (*1*, *2*) and is the apparent source of the North American tektite strewn field (*3*, *4*). This late Eocene structure [~35.4 million years ago (Ma)] is buried beneath the southern part of Chesapeake Bay, its surrounding landmasses, and the adjacent part of the continental shelf by several hundred meters of post-impact sediments (Fig. 1). The intensely disrupted, 35- to 40-km-wide central crater (collapsed transient cavity) of the structure is surrounded by a less disrupted annular trough of ~25 km radial width, thereby forming a structure with a diameter of 85 to 90 km (*1*, *2*).

The CBIS event is particularly important for understanding wet-target impact processes. The target consisted of three layers of differing strength: (i) a continental-shelf water column, (ii) water-saturated Cretaceous and Tertiary sediments, and (iii) the upper few kilometers of continental crust, composed of pre-Mesozoic igneous and metamorphic silicate rocks. These target characteristics played important roles in producing the ultimate shape, size, and internal stratigraphy of the CBIS (*5*).

Three coreholes were drilled into the CBIS in 2005 and 2006 to a composite depth of 1.76 km at Eyreville Farm, in Northampton County, Virginia, USA (Figs. 1 and 2) (*6*). The drill site is located within the central crater, ~9 km from the structure's center. Here we describe the cores and discuss what they reveal about the geologic, hydrologic, and biologic consequences of a large terrestrial impact.

Crater-fill units. The cored section of crater-fill materials consists of five major units (Fig. 2). The lowest consists of 215 m of fractured mica schist intruded by pegmatite and coarse granite (1766 to 1551 m). These pre-Mesozoic target rocks record impact effects and a pre-impact tectonometamorphic history under retrograde amphibolite-to-greenschist facies conditions.

The schists are well foliated and consist of muscovite, biotite, quartz, and plagioclase with smaller amounts of graphite, fibrolitic sillimanite, pyrite, and (locally) garnet. Interlayers include minor muscovite-biotite-quartz-plagioclase gneiss, mylonitic schist and gneiss with secondary mineralization, sparse amphibolite and epidosite, and rare tourmalinite. The granite pegmatite grades texturally into the coarse-grained granite; both consist of microcline, plagioclase, and quartz, smaller amounts of muscovite, and sporadic occurrences of biotite and garnet. The pegmatite and granite are locally discordant to foliation in the schist, but in other places they are overprinted by mylonitic deformation.

Centimeter- to meter-thick dikes of impact-generated polymict lithic breccias and suevites are locally present. The dike rocks contain sparse shock-deformed clasts and, in the case of the suevites, impact-melt particles. These materials record a wide range of shock pressures, from <10 GPa (planar fractures only) to >45 GPa (impact melt). However, except near one breccia dike, convincing evidence of shock metamorphism is lacking in the schist, pegmatite, and granite.

Brittle cataclastic deformation is unevenly overprinted on these rocks. This cataclasis could be related, at least in part, to the impact event, as indicated by fractures associated with the impact-breccia dikes. Some narrow veins that are now completely altered to secondary mineral assemblages (but may represent original melt veins) also are offset by microfault networks, indicating that fault displacements continued after emplacement of these veins.

Above the lowest unit, 154 m of suevitic (melt-bearing) and lithic impact breccias are present (1551 to 1397 m). The lower half of this section is melt-poor and contains boulders of cataclastic rock. Suevites with an average 20 to 30% by volume of melt particles are present in the upper half. They contain mineral and lithic clasts that exhibit all stages of shock metamorphism. Clast-rich impact-melt rocks (clasts in melt matrix) are locally present. The upper few meters of this unit contain impact-melt fragments with distinct shard shapes.

Numerous mineralogic features record the wide range of shock deformation in this unit. Quartz grains show a variety of shock effects, including one and (rarely) two sets of planar fractures (PFs), planar deformation features (PDFs, one or two sets, some decorated with fluid inclusions), and a common "toasted" (brown-stained) appearance. Ballen quartz (crackled devitrification texture) occurs in some melt-rich samples (*7*). Rare feldspar grains with PDFs and mica with kink banding also are present. On average, ~15% of all quartz grains are shocked (PFs and/or PDFs). The amount of melt clasts in individual suevite samples varies widely, from 1 to 77% by volume.

A 26-m-thick unit of gravelly quartz sand and large rock clasts is present at 1397 to 1371 m, just above the suevitic rocks. The base of this sand marks a transition from nearly in-place materials to overlying transported materials (Fig. 2). The rock clasts include a 13-m amphibolite block near the center of the unit, as well as single cataclasite (3.0 m) and suevite (0.4 m) boulders near the base. Gravel-sized, altered melt clasts are present at the base of the sand. The basal boulders and melt clasts are interpreted to be rip-up material from the underlying unit.

A transported, 275-m-thick granitic megablock at 1371 to 1096 m overlies the sand unit (Fig. 2). Four varieties of granite are distinguished on the basis of composition and texture, including gneissic biotite granite, fine-grained biotite granite, medium- to coarse-grained biotite granite, and red altered granite (*7*). Mica foliation is variably developed, and the granites range from foliated to massive. Xenoliths of well-foliated biotite-amphibole gneiss are present but sparse. Two granite samples have been dated at ~615 Ma (Neoproterozoic) and ~254 Ma (Permian), respectively, by the sensitive high-resolution ion microprobe (SHRIMP) U-Pb zircon method (*7*), and granites of similar ages are present elsewhere in the target region (*8*). Fractures and veins in the granite are not unusually abundant, nor are they coated or filled with impact-generated material. Also, no convincing evidence for shock metamorphism was found in the granite.

The uppermost and thickest crater-filling unit (652 m) consists of brecciated target sediments and polymict, sediment-dominated breccias (Fig. 2). The lowest part of this unit (1096 to 867 m) consists of Cretaceous nonmarine sands and clays from the

[1]U.S. Geological Survey, Reston, VA 20192, USA. [2]Department of Lithospheric Research, Center for Earth Sciences, University of Vienna, Althanstrasse 14, Vienna A-1090, Austria. [3]Department of Geological Sciences, Rutgers University, 610 Taylor Road, Piscataway, NJ 08854, USA. [4]Museum of Natural History (Mineralogy), Humboldt-University Berlin, Invalidenstrasse 43, Berlin 10115, Germany. [5]Centre for Earth, Planetary, Space, and Astronomical Research, Open University, Milton Keynes MK7 6AA, UK.

*To whom correspondence should be addressed. E-mail: ggohn@usgs.gov

lower part of the target sediment layer that are present as clasts (pebbles to ~17 m) and as matrix between those clasts. Many of the clasts display well-preserved Cretaceous stratification. Common structureless sand layers (clasts?) and sparse sand dikes indicate local sand liquefaction and fluidization. The interval above (867 to 618 m) also consists primarily of clasts and matrix derived from the Cretaceous nonmarine target sediments. However, intercalated centimeter- to meter-thick zones of Cretaceous nonmarine-sediment clasts in an unstratified, unsorted, fossiliferous, muddy, quartz-glauconite sand and granule matrix are present at the bottom (867 to 861 m) and near the top of this interval. The highest interval (618 to 444 m) consists primarily of nonmarine-sediment clasts in glauconitic matrix, with the addition of sparse shocked rock and mineral clasts and melt particles. The presence of abundant glauconite grains in these intervals represents mixing of Cretaceous and Tertiary marine sediments from the upper part of the target sediment layer with Cretaceous nonmarine sediments from the lower part.

Impact processes. The crater-fill section recovered in the Eyreville cores provides a substantial basis for interpreting the characteristics and sequence of cratering processes (Fig. 3). The near-absence of shock metamorphism in the basal schist-pegmatite-granite unit is inconsistent with its position 9 km distant from the crater's center (0.4 to 0.5 transient-crater radii). From shock barometry and attenuation studies in other craters with crystalline targets, average shock pressures of ~10 GPa or greater are expected at this location (*9*). This observation suggests that the corehole did not reach the presumably shocked in situ crater floor, but instead sampled basement-rock blocks that slumped from higher on the transient-cavity wall toward the center of the cavity.

Some of the brittle cataclasis observed in these rocks may have occurred when the strongly attenuated shock wave and subsequent release wave passed through them. Growth and coalescence of fractures into larger shear zones likely occurred when these rocks became involved in the target flow field. This initial outward- and upward-directed shearing during growth of the transient cavity (Fig. 3A) was succeeded by centrally inward- and downward-directed motion. At the beginning of inward slumping, ~40 s after impact (*5*), the basement-derived blocks were not loaded by a sedimentary cover. The resulting lack of overburden pressure allowed dilatancy, resulting in the opening of fractures and the emplacement of the lithic and suevitic dike breccias (Fig. 3B).

The suevitic and lithic breccias above the schist-pegmatite-granite unit must have been emplaced before the arrival of the overlying unshocked rock and sediment breccias (Figs. 2 and 3), which occurred on the order of 6 to 8 min after the impact (*5*) (Fig. 3C). The apparently short time available for the transportation and deposition of the suevitic and lithic breccias suggests that most of this material never left the transient cavity but was emplaced by base surging along the surface of the cavity. The breccias at depths of 1551 to 1474 m show no signs of aerodynamic transport; they consist of meter-sized lithic blocks and interlayered melt-poor suevites that support the ground-surge scenario (*10*). However, the uppermost suevite section contains shard-like melt particles, indicating airborne quenching typical of ejecta-plume deposits (*11*).

Airborne materials that were thrown high into the atmosphere and fell back later than ~6 to 8 min after impact were mixed into the stratigraphically higher sediment-dominated breccias (Fig. 2). Shock-deformed lithic clasts and melt fragments occur throughout the upper part of these breccias (618 to 444 m); melt clast–enriched horizons occur as high as 458 m depth, only 14 m below the transition to background sedimentation conditions (Fig. 3D). Thus, late ejecta-plume fallback was coeval with late-stage gravitational collapse of the transient cavity and ocean resurge (water flowing back into the cavity) (Fig. 2).

The late-stage collapse of the transient-cavity wall was achieved by mass wasting that preceded and accompanied resurge of the oceanic water column back into the cavity (Fig. 2), which occurred ~7 to 15 min after impact (*5*) (Fig. 3, C and D). The relatively undeformed and unshocked granite megablock (Fig. 2) must have originated outside the shocked crater-floor zone. Possible locations include the rim of the transient cavity, or adjacent areas outside the cavity, which were strongly affected by gravity-driven collapse and by the erosion and transport of materials by ocean resurge. In this scenario, the 275-m-thick megablock was transported at least 5 km, from ~14 km radial distance to its present position at 9 km radial distance, probably within ~6 to 10 min after impact (Fig. 3, C and D). The thin, presumably water-saturated sand layer below the granite may have facilitated this transport.

The abundant preservation of primary stratification in the weakly indurated and brecciated Cretaceous sediments (1096 to 618 m) above the granite suggests transport in a zone of low and/or spatially localized shear stress. The absence of fallback clasts

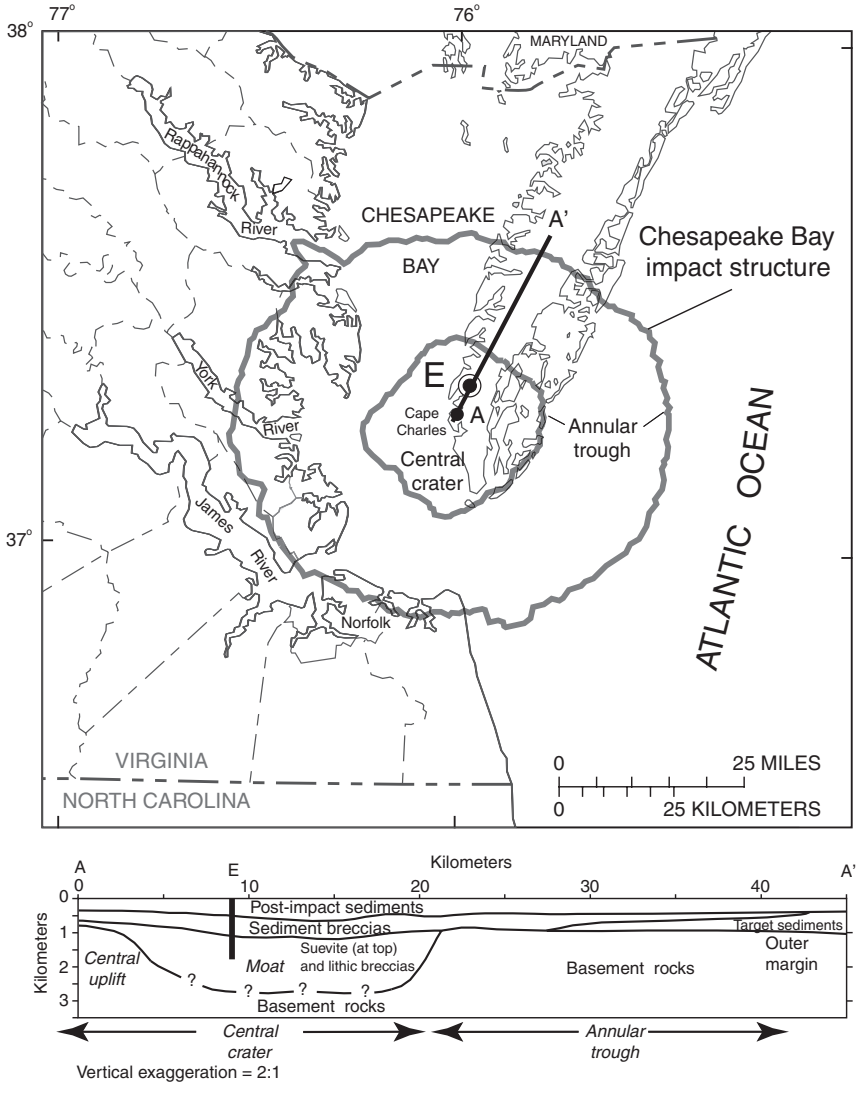

Fig. 1. Location of the Eyreville drill site (E) in the Chesapeake Bay impact structure and generalized radial cross section of the structure. The location of cross section A-A′ is shown on the map.

(shocked-rock and melt particles) in this material suggests rapid movement of a large mass of sediments. Collectively, these characteristics suggest rapid mass transport and deposition as a rock avalanche from the rim of the transient cavity.

The presence of the brecciated Cretaceous sediments directly above the granite megablock mimics the target stratigraphy where Cretaceous nonmarine sediments nonconformably overlie pre-Mesozoic igneous and metamorphic rocks. This "ghost stratigraphy" suggests the possibility that the granite and sediment section from 1397 to 618 m depth in the core moved as a single, huge, rock avalanche. The avalanche base is not at the top of the granite megablock, as shear-induced basal features (e.g., substrate folds, mixed substrate and breccia) are not present there. The avalanche base probably is the base of the thin sand below the granite at 1397 m depth, where clasts are reworked from the underlying suevitic and lithic breccias.

The glauconitic sediment-dominated breccias at 618 to 444 m represent the main pulse of ocean-water resurge into the collapsing transient cavity (Figs. 2 and 3D). The unsorted, unstratified, dominantly matrix-supported character of these deposits suggests transport and deposition by large sediment-gravity (debris) flows. The presence of glauconite represents the scouring and entrainment of Cretaceous and Tertiary marine sediments from outside the transient cavity by the resurge flow. The incorporation and dispersion of shocked-rock clasts and melt particles in the resurge indicates the persistence and collapse of the ejecta plume at this stage. A 6-m-thick zone of Cretaceous clasts in glauconitic matrix within the avalanche deposits at 867 to 861 m indicates that early ocean resurge overlapped, and likely facilitated, the gravitational collapse of the transient-cavity wall (Figs. 2 and 3D).

Vertical variations in clast types, sizes, and abundance (618 to 444 m) may indicate various stages of resurge, including inward resurge, outward anti-resurge, and oscillating "swash." The uppermost ~6 m of crater-fill sediments display stratification and size sorting that marks the transitional return to normal shelf sedimentation.

Post-impact sedimentation and tectonics. The Eyreville cores provide a high-resolution (~1 million years) chronostratigraphic record for the post-impact sediment sequences above the CBIS central crater that allows their placement into a regional depositional framework (Fig. 4). Excess accommodation space in the annular trough resulted from compaction of impact-generated materials during the first 7 million years after impact (35.4 to 27.5 Ma) (*12*). Backstripping (accounting for the effects of compaction and sediment loading) indicates that the trough was then uplifted by 50 to 125 m (27.5 to 18 Ma) (*12*). The Eyreville cores show that compaction of impact-generated materials continued to influence sedimentation above the central crater throughout the past 35.4 million years.

Most of the post-impact sequences are thinner outside the CBIS (at Tasley) than correlative sequences above the annular trough (at Exmore) (Fig. 4); previous work revealed similar lithostratigraphic trends (*13*). Sequences thicken even more above the crater moat (at Eyreville) but thin substantially above the central uplift (at Cape Charles). These changes in accommodation are due to differential compaction of variable thicknesses of impact-generated materials in the crater moat (>1000 m thick at Eyreville) versus the annular trough (~100 to 200 m thick at Exmore) and the central uplift (~300 m thick at Cape Charles). Seismic profiles across the CBIS (*1*) show numerous compaction faults offsetting post-impact sediments that dip into and thicken into the crater (*12*), supporting our interpretation.

Eustasy also influenced sedimentation in the CBIS. Eustatic control on sequence boundaries outside the structure (New Jersey–Delaware) is shown by a nearly one-to-one correspondence with ice volume increases inferred from oxygen isotopic changes from the Oligocene through the late Miocene (*14*–*16*). These sequences can be correlated to Tasley with the use of geophysical logs, and many are identified within the CBIS (Fig. 4), indicating eustatic influence.

However, there are also differences due to regional and impact tectonism. For example, Oligocene (~33 to 24 Ma) sequences are relatively thin to absent inside the central crater, in contrast to sections in the annular trough and outside the crater to the north (Fig. 4). The presence of a thick Oligocene section at Langley (Fig. 4, annular trough) argues for sediment starvation of the central crater, whereas the presence of a thick Oligocene section in New Jersey implicates regional tectonics. Lower Miocene sequences C1 to C5 (~24 to 17 Ma) are thin to absent inside the CBIS, in contrast to sections to the north (Fig. 4). Mid-Miocene sequences C6 to C8 (~16 to 13 Ma) are thick at Eyreville and Exmore but are thin or absent at Langley, most likely reflecting uplift of the Norfolk arch (*17*); mid-upper Miocene sequences C9 and C10 (~12 to 10 Ma) extend across the Delmarva Peninsula and are recovered at Exmore but are absent in the central crater and to the south, indicating regional uplift possibly coupled with low sedimentation rates. The preservation of uppermost Miocene to Pliocene (~7 to 2 Ma) sequences within the crater and regions to the south, versus their absence or nonmarine nature to the north, is attributed to excess regional subsidence of Virginia–North Carolina relative to New Jersey–Delaware.

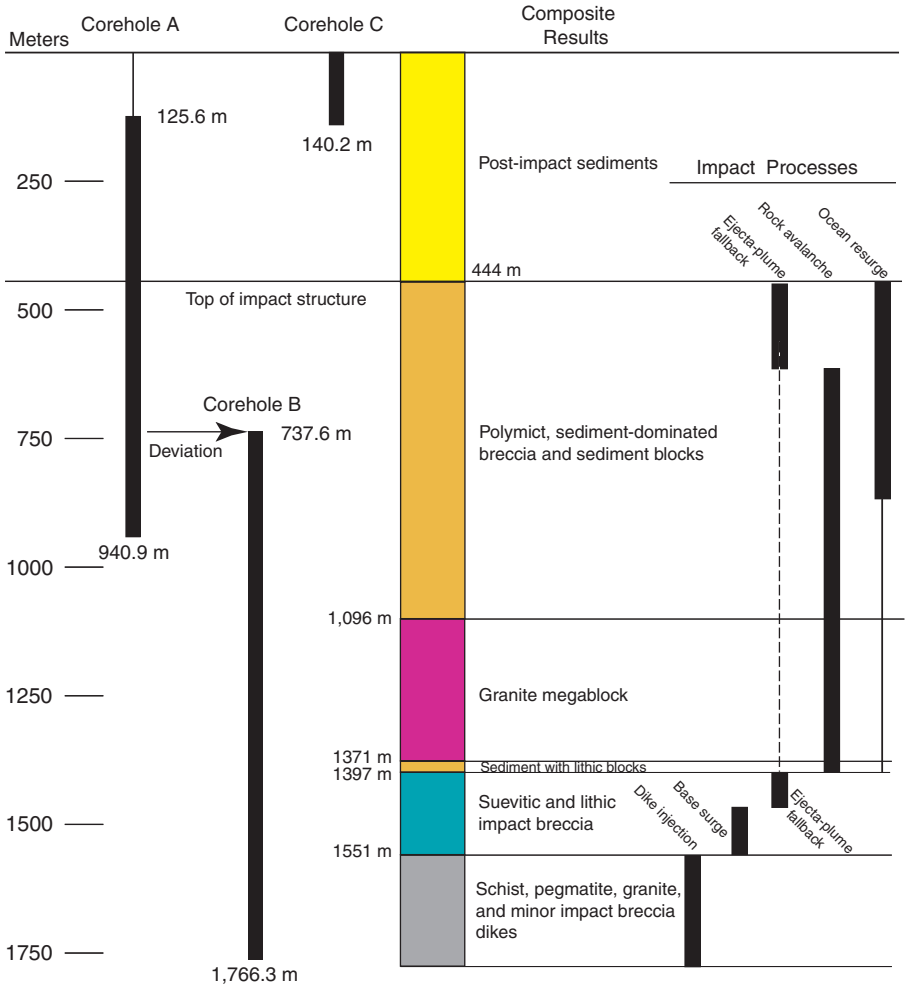

Fig. 2. Corehole depths, cored intervals, geologic column, and inferred impact processes for the A, B, and C coreholes at the Eyreville drill site. Intervals affected by selected impact processes are indicated.

Periods of uplift and excess subsidence at a scale of tens of meters in 1 to 3 million years (*16*) overprint subsidence from simple lithospheric cooling, flexure, and impactite compaction. We suggest that uplift and excess subsidence was caused by regional differential movement of fault-bounded basement blocks in response to variations in intraplate stress.

Hydrologic consequences. The CBIS is colocated with an inland extension of salt water in the coastal aquifers of Virginia (*13*) near population centers that rely heavily on groundwater. In addition, brine (*18*) with salinity exceeding that of seawater was detected at other borehole locations inside the CBIS (*19*, *20*). A recent analysis shows that hydraulic conditions within the CBIS would not have allowed groundwater to be flushed out since the time of impact (*21*). Thus, the brine likely is a residual from early post-impact hydrothermal boiling (*22*) or some other impact process.

In the Eyreville core, pore waters change from fresh to salty between depths of 100 and 440 m within the post-impact section (Fig. 5A). The monotonic trend in salinity suggests that molecular diffusion is a dominant process with little lateral advection of groundwater since the impact. Below 300 m, core samples containing brine with salinities up to twice that of seawater extend down to 1000 m. The brine in the breccias is too voluminous to be from hydrothermal boiling in the suevite layer (*23*), which suggests that it existed within the target sediments before impact; similar deep brine occurs north and south of the CBIS today (*24*, *25*). The local salinity variability and minima between 500 and 800 m could be inherited from the sediment clasts, or it could have been a zone of flushing during recent low sea levels. However, the salinity minima in this zone correlate with clay-rich sediments in the core, suggesting a connate rather than a recent seawater or meteoric origin, because flushing would tend to focus less saline water through the coarse-grained sediments. The evidence indicates that most of the groundwater currently in the CBIS survived the impact and has never been flushed out. Sluggish hydraulic conditions (*21*) would delay the migration of brine toward the population centers.

Effects on deep subsurface biota. The CBIS core provided microbiological samples from the deep terrestrial subsurface. Robust protocols were used to prevent and monitor contamination during recovery of samples (*26*). Samples were obtained at intervals of ~30 m for enumeration (Fig. 5B) and at intervals of ~60 m for culture and molecular biologic investigations.

Microbial abundance declines logarithmically from the surface across the transition from the post-impact sediments to the sediment breccias to near the middle of those breccias at a depth of ~800 m. This decline is steeper than that typical of many deep marine sediments covering a similar distance and geologic time interval (late Eocene to present), although near-surface abundances are similar (*27*–*29*). This observation could be related to more rapidly declining available carbon at depth relative to the deep marine biosphere and/or increasing salt concentration. Salinity concentrations substantially exceeding that of seawater (Fig. 5A) would limit the diversity and abundance of microorganisms capable of growing (*30*).

In the lower part of the sediment breccias (1096 to 867 m), salinity peaks at 65% and no cells were detected with our methodology except in two locations (samples collected from a mixed-clast region just above clay boulders at 1064 to 1025 m). The permeability of this section is generally low, and water within the section is likely a relict of the immediate post-impact environment. Our data are consistent with a scenario that includes sterilization of the section by impact-generated heat (either directly or as a result of vertically advected heat from the suevites and impact-melt rocks) (*22*) and high salinity that has limited microbial recolonization. Thus, most of this interval may have remained biologically impoverished since the impact.

The abundance of cells markedly increases below the granitic megablock, corresponding to the region of suevite and associated lithic breccias and the region of crystalline-rock blocks (1766 to 1397 m). The interval from 1424 to 1397 m consists of 20 to 30% impact-melt clasts with a suggested average temperature at the time of deposition of >350°C on the basis of numerical calculations used for modeling thermal maturity (*31*). This clearly exceeds the upper limit for growth and the accepted sterilization temperature for most microorganisms (>121°C steam or

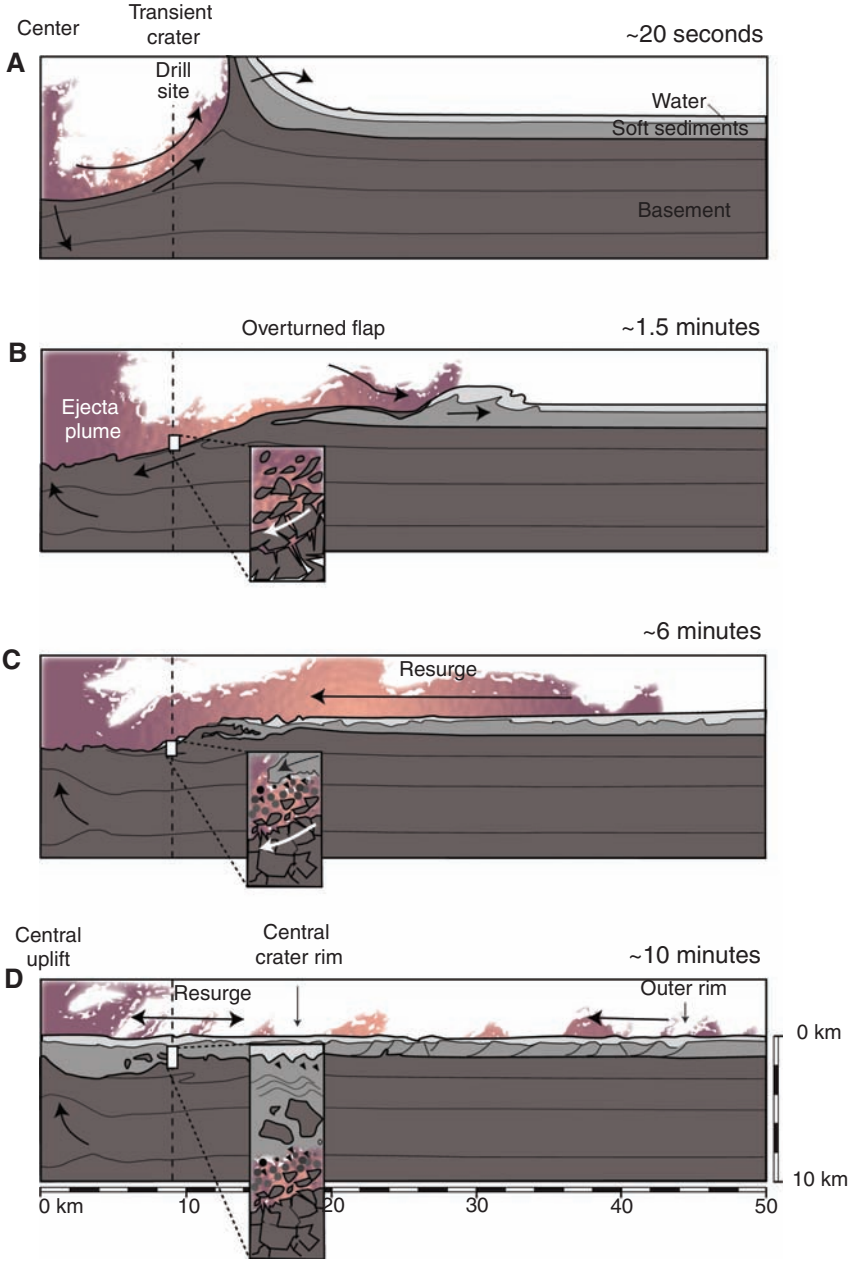

Fig. 3. Diagram illustrating the processes and history of crater collapse in four stages, (**A**) to (**D**). The close-ups illustrate the cratering processes at the corehole location. [Modified from (*5*)]

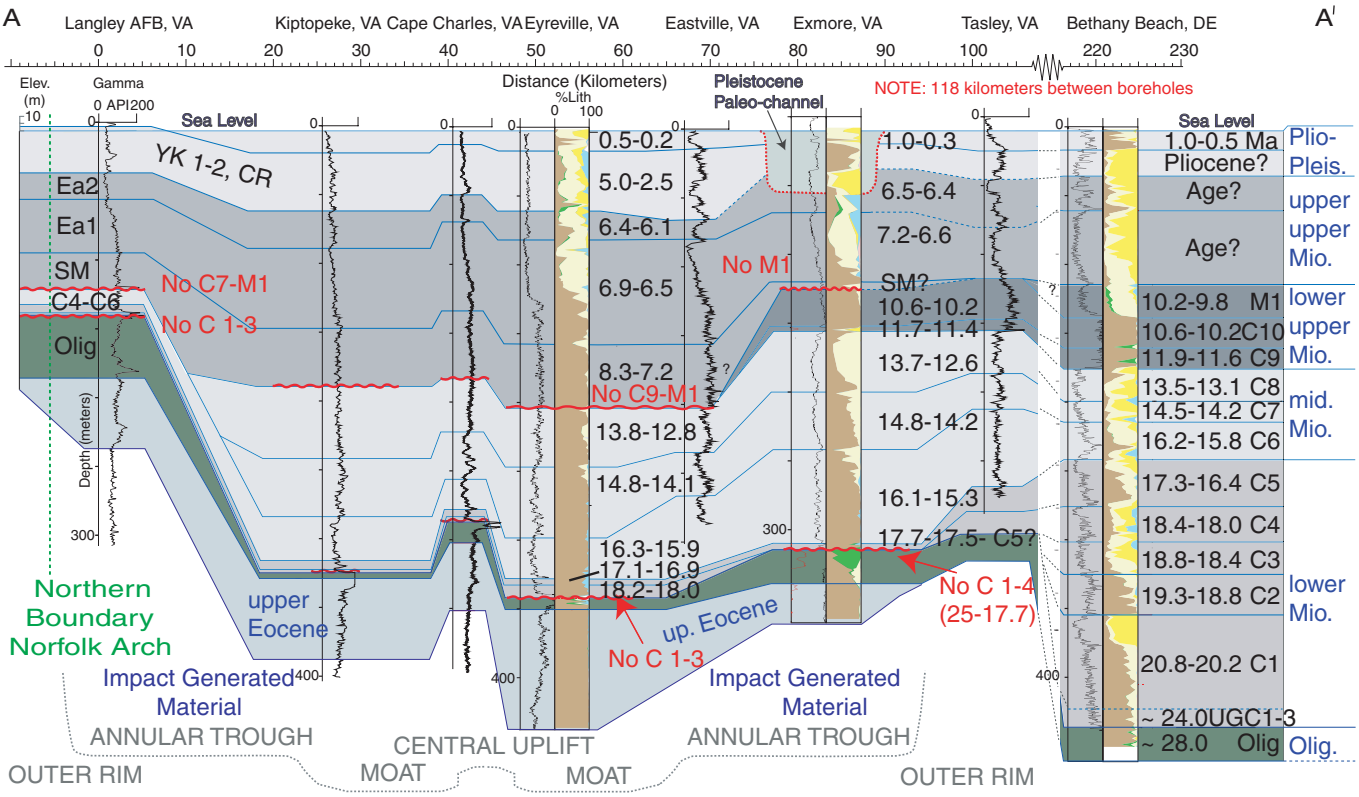

Fig. 4. Corehole and well log cross section, Langley, Virginia, to Bethany Beach, DE. Bethany Beach (*16*), Langley, Kiptopeke, Cape Charles, and Exmore are coreholes; Eastville and Tasley are water wells with gamma-ray logs; sequence ages are based on age-depth plots primarily using Sr isotopes. Sequences C1 to C10 and M1 are defined at Bethany Beach (*16*); YK, Ea1, Ea2, CR, and SM are defined at Eyreville. Blue lines represent sequence boundaries; wavy red lines indicate coalesced sequence boundaries where one or more sequences are absent. Lithologic columns: bright yellow, coarse quartz sand; pale yellow, fine quartz sand; blue, carbonate sand; brown, silt and clay; green, glauconite sand; pink-white, mica or other. See fig. S10 for location of cross section A-A′.

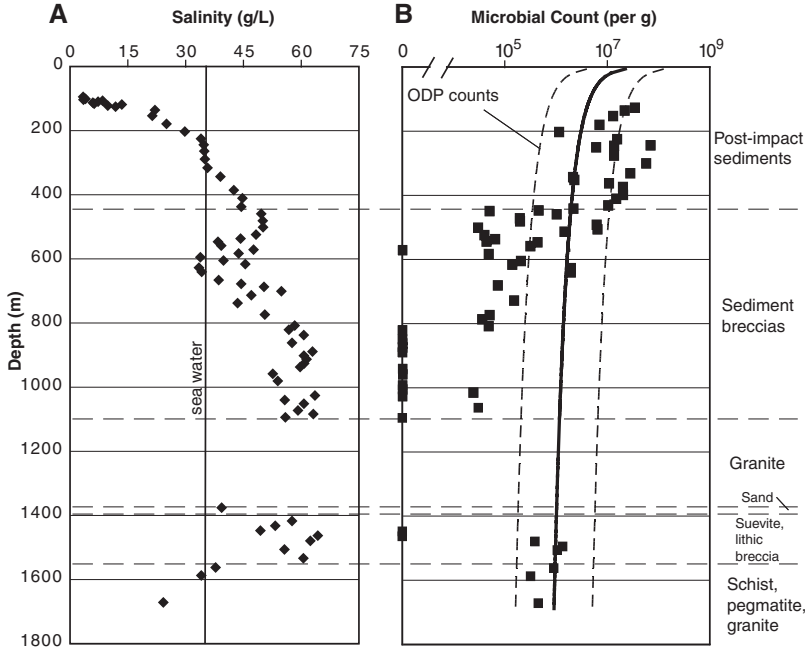

Fig. 5. (**A**) Profile of salinity at the Eyreville drill site, based on pore water extracted from core samples. (**B**) Microorganism count per gram dry weight. Counts are compared to average Ocean Drilling Program (ODP) microorganism data regression (*29*). The ODP regression lines were corrected assuming a conversion factor of 1.3 ml of sediment per gram. The correction factor was calculated by measuring 1 ml of 20 representative samples throughout the core and obtaining the dry weight of sediment. All values were within 10% of the mean.

>160°C dry heat). Microorganisms were reintroduced at some point after ambient temperatures dropped below the upper temperature limit for microbial growth (121°C) (*32*). The widespread presence of fractures in the crystalline rocks suggests that impact and post-impact processes could have contributed to the movement of fluids and perhaps organisms into this deeper region.

Understanding how impacts have influenced the characteristics of the deep subsurface is important for gaining insight into the biological potential of the deep biosphere during the Archean, when the impact flux was higher, as well as the biological potential of the deep biosphere on Mars, where impacts have had a profound influence on surface and subsurface geology. Data from the CBIS suggest that impact events can disrupt the deep subsurface biosphere. Although detrimental effects may be caused by a biologically sterilizing pulse, subsequent recolonization (and even enhanced growth) might occur if reorganization and restructuring of the lithologic units (including fracturing), and/or inundation of the subsurface with seawater and terrestrial materials that potentially introduce fresh electron acceptors and donors, lead to the establishment of a suitable environment.

References and Notes

1. C. W. Poag, C. Koeberl, W. U. Reimold, *The Chesapeake Bay Crater, Geology and Geophysics of a Late Eocene Submarine Impact Structure* (Springer, Berlin, 2004).

2. J. W. Horton Jr., D. S. Powars, G. S. Gohn, Eds., *U.S. Geol. Surv. Prof. Pap. 1688* (2005).
3. C. Koeberl, C. W. Poag, W. U. Reimold, D. Brandt, *Science* **271**, 1263 (1996).
4. A. Deutsch, C. Koeberl, *Meteorit. Planet. Sci.* **41**, 689 (2006).
5. G. S. Collins, K. Wünnemann, *Geology* **33**, 925 (2005).
6. G. S. Gohn *et al*., *Eos* **87**, 349 (2006).
7. J. W. Horton Jr. *et al*., *Geol. Soc. Am. Abstr. Prog.* **39**, 451, abstract 167-5 (2007).
8. J. W. Horton Jr., J. N. Aleinikoff, M. J. Kunk, C. W. Naeser, N. D. Naeser, *U.S. Geol. Surv. Prof. Pap. 1688* (2005).
9. P. B. Robertson, R. A. F. Grieve, in *Impact and Explosion Cratering: Planetary and Terrestrial Implications*, D. J. Roddy, R. O. Pepin, R. B. Merrill, Eds. (Pergamon, New York, 1977), pp. 687–702.
10. A. Wittmann, T. Kenkmann, L. Hecht, D. Stöffler, *Geol. Soc. Am. Bull.* **119**, 1151 (2007).
11. D. Stöffler *et al*., *Meteorit. Planet. Sci.* **39**, 1035 (2004).
12. T. Hayden *et al*., *Geology* **36**, 327 (2008).
13. D. S. Powars, T. S. Bruce, *U.S. Geol. Surv. Prof. Pap. 1612* (1999).
14. K. G. Miller, G. S. Mountain, Leg 150 Shipboard Party, Members of the New Jersey Coastal Plain Drilling Project, *Science* **271**, 1092 (1996).
15. K. G. Miller *et al*., *Science* **310**, 1293 (2005).
16. J. V. Browning *et al*., *Geol. Soc. Am. Bull.* **118**, 657 (2006).
17. D. S. Powars, *U.S. Geol. Surv. Prof. Pap. 1622* (2000).
18. C. W. Poag, *The Chesapeake Invader* (Princeton Univ. Press, Princeton, NJ, 1999).
19. E. R. McFarland, T. S. Bruce, *U.S. Geol. Surv. Prof. Pap. 1688-K* (2005).
20. W. E. Sanford *et al*., *Eos* **85**, 369 (2004).
21. W. E. Sanford, *J. Geochem. Explor.* **78–79**, 243 (2003).
22. W. E. Sanford, *Geofluids* **5**, 185 (2005).
23. See supporting material on *Science* Online.
24. L. Radford, L. B. Cobb, R. L. McCoy, *U.S. DOE Rep. DOE/ET/28373-1* (1980).
25. F. T. Manheim, M. K. Horn, *Southeast. Geol.* **9**, 215 (1968).
26. A. L. Gronstal *et al*., *Geol. Soc. Am. Abstr. Prog.* **39**, 316, abstract 116-22 (2007).
27. R. J. Parkes *et al*., *Nature* **371**, 410 (1994).
28. S. D'Hondt *et al*., *Science* **306**, 2216 (2004).
29. R. J. Parkes, B. A. Cragg, P. Wellsbury, *Hydrogeol. J.* **8**, 11 (2000).
30. W. D. Grant, *Philos. Trans. R. Soc. London Ser. B* **359**, 1249 (2004).
31. M. L. Malinconico, W. E. Sanford, J. W. Horton Jr., abstract for Conference on Large Meteorite Impacts and Planetary Evolution IV, Vredefort Dome, South Africa, abstract 3068 (2008).
32. K. Kashefi, D. R. Lovley, *Science* **301**, 934 (2003).

33. The International Continental Scientific Drilling Program, the U.S. Geological Survey, and the NASA Science Mission Directorate provided funding for the drilling project. NSF and the Austrian Science Foundation provided supplementary funding for the drill-site operations. DOSECC Inc. conducted the administrative and operational management of the deep drilling project. We thank the Buyrn family for use of their land as a drilling site, the scientific and technical staff of the Chesapeake Bay Impact Structure Drilling Project for their many contributions, A. Gronstal (Open University, UK) for the microbe enumeration data, L. Edwards (USGS) for discussions of the post-impact geology, and G. Collins (Imperial College, UK) and K. Wünnemann (Humboldt-University Berlin) for making available the results of their numerical modeling.

Supporting Online Material

www.sciencemag.org/cgi/content/full/320/5884/1740/DC1
Materials and Methods
Figs. S1 to S10
Table S1
References

4 April 2008; accepted 28 May 2008
10.1126/science.1158708

Dislocation Mean Free Paths and Strain Hardening of Crystals

B. Devincre,[1] T. Hoc,[2] L. Kubin[1]*

Predicting the strain hardening properties of crystals constitutes a long-standing challenge for dislocation theory. The main difficulty resides in the integration of dislocation processes through a wide range of time and length scales, up to macroscopic dimensions. In the present multiscale approach, dislocation dynamics simulations are used to establish a dislocation-based continuum model incorporating discrete and intermittent aspects of plastic flow. This is performed through the modeling of a key quantity, the mean free path of dislocations. The model is then integrated at the scale of bulk crystals, which allows for the detailed reproduction of the complex deformation curves of face-centered cubic crystals. Because of its predictive ability, the proposed framework has a large potential for further applications.

Dislocations are complex defects of crystalline materials, which have been investigated for more than 70 years. Their fundamental and economical importance arises from the number of properties they govern, such as the high strength of nanostructured materials, the reliability of semiconductor devices, the processing and service life of structural materials, or the rheological properties of tectonic events in Earth's crust.

The irreversible, or plastic, deformation of crystals results from the motion on crystallographic planes of linear defects, the dislocations (*1*, *2*). These defects carry an elementary amount of shear (the Burgers vector) that is usually the smallest translation of the crystal lattice. During plastic flow, dislocations multiply and their mutual interactions hinder their motion. As a consequence, a shear stress increase $d\tau$ has to be imposed to produce a shear strain increase $d\gamma$. By definition, the ratio $d\tau/d\gamma$ is the strain hardening rate. Although dislocation theory has successfully explained many aspects of the strength of crystalline solids, predicting strain hardening is "the most difficult remaining problem" (*3*). The present dislocation-based models for strain hardening still have difficulties integrating elementary dislocation properties into a continuum description of bulk crystals or polycrystals. As a consequence, current approaches cannot avoid making use of extensive parameter fitting.

The present work takes advantage of three-dimensional dislocation dynamics (DD) simulations (*4*–*8*) for averaging dislocation properties at the intermediate scale of slip systems, which are ensembles of dislocations having the same Burgers vector and slip plane. The use of periodic boundary conditions allows for the tayloring of large dislocation glide paths and the investigation of volumes that are representative of the bulk material (*4*). One can then derive a continuum formulation on the basis of physically justified mechanisms and parameters, and this formulation is further integrated at the scale of a bulk crystal. Face-centered cubic (fcc) crystals are taken as benchmark materials because of their well-documented, but rather complicated, stress/strain response.

We started by considering the critical stress τ_c^i for the activation of slip system i as a function of the dislocation densities ρ^j stored (i.e., temporarily or permanently immobilized) in all slip systems j. This critical stress is given by a generalized Taylor relation (*9*) of the form, $\tau_c^i = \mu b \sqrt{\sum_j a_{ij} \rho^j}$, where μ is the shear modulus and b the modulus of the Burgers vector. In fcc crystals, the symmetric tensor a_{ij} contains six independent dimensionless coefficients, which account for the average strength of pair interactions between slip systems that result from short- and long-range interactions. Their values were recently determined from DD simulations (*5*).

For determining strain hardening, the key quantity is the rate at which the critical stress evolves with strain or, equivalently, the rate at which dislocations accumulate under strain. For this purpose, it is useful to define a dislocation mean free path L, which is the distance traveled by a dislocation segment of length l before it is stored by interaction with the microstructure. When the line moves by a distance dx, it sweeps an area ldx and produces a shear strain $d\gamma = bldx/V$, where V is the volume of the crystal. The stored density has then statistically increased by $d\rho = (dx/L)l/V$, and the incremental storage rate is $d\rho/d\gamma = 1/bL$. This definition is only valid in differential form, as dislocation lines multiply when they move. Following Kocks *et al*. and

[1]Laboratoire d'Etude des Microstructures, Unité Mixte de Recherche (UMR) 104 CNRS, CNRS–Office National d'Etudes et de Recherches Aérospatiales (ONERA), 20 Avenue de la Division Leclerc, BP 72, 92322 Chatillon Cedex, France. [2]Laboratoire MSSMat, UMR 8579 CNRS, Ecole Centrale Paris, Grande Voie des Vignes, 92295 Chatenay-Malabry Cedex, France.

*To whom correspondence should be addressed. E-mail: ladislas.kubin@onera.fr